Simplified theory of double-sided linear induction motor with squirrel-cage elastic secondary

J.F. Gieras, Ph.D., D.Sc.

Indexing terms: *Induction motors, squirrel-cage secondaries*

Abstract: The theoretical analysis, the method of calculation and the experimental tests on a double-sided linear induction motor (DLIM) with squirrel-cage secondary member are given. The air-core secondary is elastic and consists of copper bars, a braided conductive lines as end rings and woven plastics filaments. Equations of two-dimensional and one-dimensional magnetic-flux-density distribution in the secondary and the airgap are derived. Formulas for resistance and reactance of the squirrel-cage secondary and the thrust of DLIM are obtained. The end effect caused by the open-endedness of the airgap is taken into account. Performance characteristics, i.e. no-load and short-circuit curves obtained from calculations and measurements, are compared.

Streszczenie: Podano analizę teoretyczną, metodę obliczeń i badania eksperymentalne dwustronnego silnika indukcyjnogo liniowego (DSIL) o klatkowej części wtórnej. Bezrdzeniowa część wtórna jest elastyczna i składa się z prętów miedzianych połączonych ze sobą na końcach linką miedzianą i przeplecionych taśmą z tworzywa sztucznego. Wyznaczono równania dwuwymiarowego i jednowymiarowego rozkładu indukcji magnetycznej w części wtórnej i szczelinie powietrznej. Na podstawie tych równań wyprowadzono zależności na rezystancję i reaktancję klatkowej części wtórnej oraz na siłę ciągu DSIL. Uwzględniono zjawiska końcowe wywołane skończoną długością rdzenia części pierwotnej. Obliczone charakterystyki biegu jałowego, obciążenia oraz zwarcia porównano z charakterystykami zmierzonymi.

List of principal symbols

A = magnetic vector potential (A_m = peak magnetic vector potential or peak line-current density), A/m
a_R = coefficient for resistance and reactive power
a_X = coefficient for reactance and reactive power
B = magnetic flux density (B_m = peak magnetic flux density), T
d = thickness of the homogeneous secondary, m
E = electric field strength (E_m = peak electric field strength), V/m
F = force, N
f = frequency, Hz
g = length of the airgap, m
I = electric current, A
k = factor for reducing the resistance and reactance of the squirrel cage to the primary system
k_w = winding factor
k_{zv} = impedance-increase factor due to transverse end effect
k_v = attenuation factor, 1/m
m = number of phases
N = number of turns per phase
N_b = number of bars
P = active power (P_e = electromagnetic power), W
p = number of pole pairs
R = resistance, Ω
s = slip
U = supply voltage, V
v = linear velocity, m/s
w = width of the secondary, m
X = reactance, Ω
Z = impedance, Ω
z = surface wave impedance,
α_v = complex propagation constant, 1/m
β_v = $v\pi/\tau$ = real constant, 1/m
ε_1 = EMF of the primary winding, V
η = efficiency
κ_v = complex propagation constant dependent on the pole pitch, 1/m
Λ_b = length of the belt (the secondary), m
μ = magnetic permeability (μ_0 = permeability of free space, μ_r = relative, μ_{re} = relative equivalent, μ_{rs} = relative surface)
v = space harmonics of field distribution along the pole pitch
σ = electric conductivity, S/m
τ = pole pitch, m
ϕ = phase angle (between current and voltage vectors), rad
ω = $2\pi f$ = angular frequency, rad/s

Paper 2782B (P1), first received 4th August 1982 and in revised form 7th March 1983

The author is with the Electrical Machines Department, Insitute of Telecommunication & Electrical Engineering, Academy of Technology & Agriculture, Pl 85-763 Bydgoszcz, Poland

1 Introduction

The double-sided linear induction motor (DLIM) with squirrel-cage secondary produces thrust by means of an interaction between the primary field and the eddy currents induced in the secondary bars. A single-sided linear induction motor with a squirrel-cage reaction rail has been tested by Eastham and Katz [1]. The thrust forces indicate that the cage-rail single-sided linear induction motor performance is similar to that traditionally associated with the conventional squirrel-cage induction motor with frequency-independent rotor resistance.

So far as the author is aware, research into DLIMs with squirrel-cage secondaries without ferromagnetic cores has not had a high priority. If the air-core squirrel-cage secondary is elastic, it would be useful in, for example, conveyor systems [2–4]. The squirrel-cage secondary is more resistant and tougher than those consisting of a homogeneous belt made of copper. The theory of DLIM with a homogeneous secondary in form of both a plate and a belt is widely known. References 5–8 contain one-dimensional and two-dimensional analyses of the electromagnetic field. References 10–12 give the three-dimensional field analysis. Accurate predictions of performances are only possible if

the field and eddy currents can be predicted with reasonable certainty. The quantitative evaluation of electromagnetic fields in the airgap is rather difficult. The main sources of difficulty are the edge effects [13–17].

The paper gives an analysis of the DLIM with an air-core squirrel-cage secondary in two stages:

(i) a two-dimensional analysis taking into account skin effects but not edge affects

(ii) a one-dimensional analysis taking into account edge effects and skin effects by substituting the secondary equivalent thickness coming from two-dimensional analysis

2 Construction of DLIM with squirrel-cage secondary

It is possible to apply DLIMs, for example, to the propulsion of belt conveyors. The DLIMs eliminate both driving gears and rotary electric motors. The model of a belt conveyor with DLIM constructed by the author is shown in Fig. 1. Design parameters for the DLIM primary, which

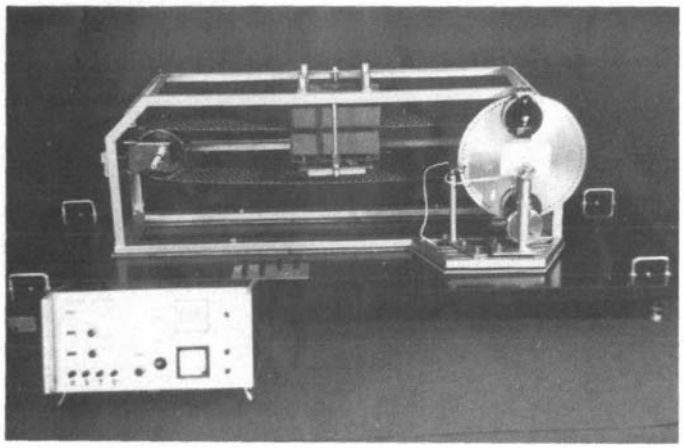

Fig. 1 *Experimental belt conveyor with DLIM*

was designed and fabricated in Poland by the Factory of Electrical Machines and Reducers 'Indukta', are given in Appendix 8.1. An elastic belt made of copper bars, a braided line consisting of copper wires and woven plastics filaments is used as the secondary. The ends of the bars are connected together by the conducting braided line and form a squirrel cage. Characteristics of the secondary are also shown in Appendix 8.1.

A squirrel cage can be imagined as a polyphase winding whose number of phases is equal to the number of pole pairs of the travelling field. When considering the squirrel cage as a polyphase winding, it should be assumed to be star connected and short circuited. Then the braided line elements resistances should be allowed for by a corresponding increase in the bar resistances. The resistance R_2 and, correspondingly, the inductive leakage reactance X_2 of the secondary should be equal to

$$R_2 = \frac{\Lambda_b}{\tau N_b}\left(R_b + 2R_c + 2R_l \frac{1}{4\sin^2(\pi/2p)}\right) \quad (1)$$

$$X_2 = \frac{\Lambda_b}{\tau N_b}\left(X_b + 2X_c + 2X_l \frac{1}{4\sin^2(\pi/2p)}\right) \quad (2)$$

where R_b = cage resistance, X_b = cage-bar reactance, R_c, X_c = resistance and reactance of contact between the bar and the braided line, R_l, X_l = resistance and reactance of a braided-line element, Λ_b = length of the conveyor belt and N_b = number of belt bars. As the secondary has no ferromagnetic core, the reactance X_2 should be considered as very small ($X_2 < R_2$, $X_2 \approx 0$). For the belt conveyor with the DLIM shown in Fig. 1 the resistance $2R_c$ = 0.00092 Ω at 20°C; this is an average value, which comes from measurements of contact resistances of all the bars. The factor for reducing the resistance and reactance of the squirrel cage to the primary system, with the number of phases of the secondary system $m_2 = 2p$, the number of turns per phase $N_2 = 0.5$ and the winding factor $k_{w2} = 1$, is given by

$$k = 2m_1(N_1 k_{w1})^2/p \quad (3)$$

where m_1 = number of the primary phases, N_1 = number of the primary-winding turns connected in series and k_{w1} = winding factor of the primary.

As the secondary has to be elastic and tensile resistant, the bars are interleaved by the woven tapes as in Fig. 2.

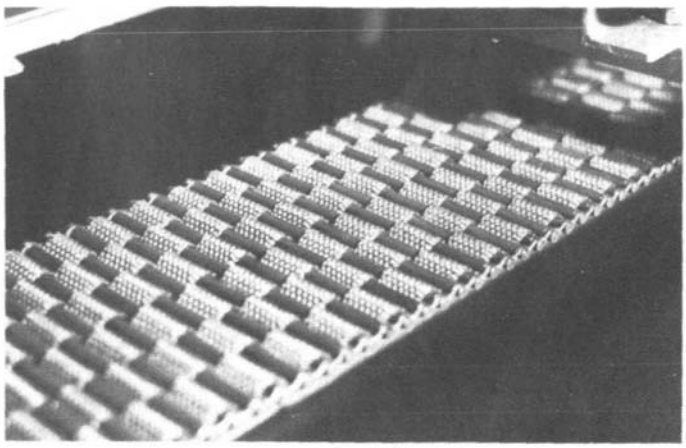

Fig. 2 *Squirrel-cage secondary of DLIM*

The electromagnetic thrust

$$F_e = P_e/2\tau f = F_m + \Delta F_m \quad (4)$$

is higher than the mechanical thrust F_m due to the mechanical force loss

$$\Delta F_m = \Delta F_m|_{s=s_0}[(1 - s)/(1 - s_0)]^n(v_0/v) \quad (5)$$

where P_e = electromagnetic power transferred from the primary to the secondary, s_0 = slip at no load, v_0 = linear velocity at no load, $\Delta F_m|_{s=s_0}$ = mechanical force loss at no load and $n \approx 3$ in case of small DLIMs.

During the tests, a braking thrust is produced by an eddy-current brake with an aluminium disc.

3 Theory

3.1 DLIM with infinite-length primary and secondary

The model chosen to represent the infinite-length double-sided linear induction machine is shown in Fig. 3. The cartesian co-ordinate system is fixed to the secondary. Equations for the two-dimensional electromagnetic field

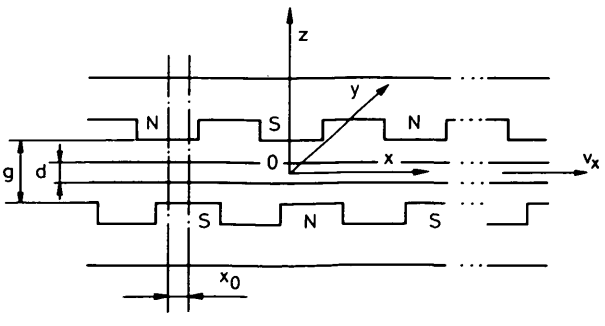

Fig. 3 *DLIM with infinite-length primary and secondary*

distribution in the secondary will be derived using the following assumptions:

(*a*) the primary is composed of thin laminations with infinite magnetic permeability and with zero electric conductivity in the *y*-direction

(*b*) the centre line of the upper inductor *N*-pole, in the general case, is displaced from the centre line of the lower inductor *S*-pole by the segment x_0

(*c*) the secondary consists of a homogeneous isotropic material of finite conductivity and magnetic permeability, and is situated symmetrically in the airgap with respect to the *x*-axis

(*d*) the active surfaces of the secondary are parallel to the active surface of the primary

(*e*) the relative equivalent magnetic permeability of the secondary is expressed by the formulas:

$$\mu_{re} = \mu_{rs}(\mu' - j\mu'') \tag{6}$$

$$\mu' = a_R a_X \tag{7}$$

$$\mu'' = 0.5(a_R^2 - a_X^2) \tag{8}$$

and the coefficients a_R and a_X take magnetic saturation and hysteresis into account [18, 19]

(*f*) the equivalent magnetic permeability of the secondary for higher harmonics of magnetic field strength is the same as for the fundamental harmonic

(*g*) the secondary currents may flow in the *y*-direction but not in the normal direction (the *z*-axis)

(*h*) the space period of electromagnetic field distribution along the pole pitch is equal to 2τ

(*i*) all quantitites vary sinusoidally with time

The equations of two-dimensional electromagnetic field distribution (Appendix 8.2) have the following form ($x_0 = 0$):

$$E_{my} = \sum_{\nu=1}^{\infty} \frac{2\omega_\nu \sinh(\kappa_\nu d/2)}{\beta_\nu \sinh(\kappa_\nu d)} B_{m\nu} \exp(-j\beta_\nu x) \cosh(\kappa_\nu z) \tag{9}$$

$$B_{mx} = -\sum_{\nu=1}^{\infty} \frac{2j\kappa_\nu \sinh(\kappa_\nu d/2)}{\beta_\nu \sinh(\kappa_\nu d)} \times B_{m\nu} \exp(-j\beta_\nu x) \sinh(\kappa_\nu z) \tag{10}$$

$$B_{mz} = \sum_{\nu=1}^{\infty} \frac{2 \sinh(\kappa_\nu d/2)}{\sinh(\kappa_\nu d)} B_{m\nu} \exp(-j\beta_\nu x) \cosh(\kappa_\nu z) \tag{11}$$

where

$$\omega_\nu = [1 - \nu(1 - s)\omega] \tag{12}$$

$$\beta_\nu = \nu\pi/\tau \tag{13}$$

$$\kappa_\nu = (\alpha_\nu^2 + \beta_\nu^2)^{1/2} = (a_{R\nu} + ja_{X\nu})k_\nu \tag{14}$$

$$\alpha_\nu = (j\omega_\nu \mu_0 \mu_{re} \sigma)^{1/2} = (a_R + ja_X)k_\nu \tag{15}$$

$$k_\nu = (\omega_\nu \mu_0 \mu_{rs} \sigma/2)^{1/2} \tag{16}$$

For the symmetrical three-phase winding of the primary $\nu = 1, 7, 13, 19, \ldots$. $B_{m\nu}$ is the peak value of the νth harmonic of the magnetic-flux-density normal component. The attenuation factor k_ν (eqn. 16) is for surface magnetic permeability. The coefficients in eqn. 15 for carbon steel are approximately $a_R \approx 1.45$, $a_X \approx 0.85$, and for nonmagnetic materials $a_R = a_X = 1$.

Other coefficients are equal to:

(i) for the ferromagnetic secondary:

$$a_{R\nu} = \frac{1}{\sqrt{2}} \left\{ \left[4a_R^2 a_X^2 + \left(a_R^2 - a_X^2 + \frac{\beta_\nu^2}{k_\nu^2}\right)^2 \right]^{1/2} + a_R^2 - a_X^2 + \frac{\beta_\nu^2}{k_\nu^2} \right\}^{1/2} \tag{17}$$

$$a_{X\nu} = \frac{1}{\sqrt{2}} \left\{ \left[4a_R^2 a_X^2 + \left(a_R^2 - a_X^2 + \frac{\beta_\nu^2}{k_\nu^2}\right)^2 \right]^{1/2} - a_R^2 + a_X^2 - \frac{\beta_\nu^2}{k_\nu^2} \right\}^{1/2} \tag{18}$$

(ii) for the nonmagnetic secondary:

$$a_{R\nu} = \frac{1}{\sqrt{2}} \left\{ \left[4 + \left(\frac{\beta_\nu}{k_\nu}\right)^4 \right]^{1/2} + \frac{\beta_\nu^2}{k_\nu^2} \right\}^{1/2} \tag{19}$$

$$a_{X\nu} = \frac{1}{\sqrt{2}} \left\{ \left[4 + \left(\frac{\beta_\nu}{k_\nu}\right)^4 \right]^{1/2} - \frac{\beta_\nu^2}{k_\nu^2} \right\}^{1/2} \tag{20}$$

Next, the DLIM with a nonmagnetic secondary will be considered, i.e. $\mu_{rs} = 1$, $a_R = a_X = 1$, $\mu' = 1$, $\mu'' = 0$.

The surface wave impedance is given by

$$\begin{aligned} z_\nu &= \mu_0 \mu_{rs} \left. \frac{E_{my\nu}}{B_{mx\nu}} \right|_{z=d/2} \\ &= \frac{j\omega_\nu \mu_0 \mu_{rs}}{\kappa_\nu} \frac{\cosh(\kappa_\nu d/2)}{\sinh(\kappa_\nu d/2)} \\ &= \frac{\alpha_\nu^2}{\sigma} \frac{1}{\kappa_\nu} \coth(\kappa_\nu d/2) \\ &= \frac{2jk_\nu^2}{(a_{R\nu} + ja_{X\nu})k_\nu \sigma} \coth(\kappa_\nu d/2) \\ &= \frac{a_{X\nu} + ja_{R\nu}}{0.5(a_{R\nu}^2 + a_{X\nu}^2)} \frac{k_\nu}{\sigma} \coth(\kappa_\nu d/2) \\ &= (A_{R\nu} + jA_{X\nu}) \frac{k_\nu}{\sigma} \coth(\kappa_\nu d/2) \end{aligned} \tag{21}$$

where

$$A_{R\nu} = \frac{a_{X\nu}}{0.5(a_{R\nu}^2 + a_{X\nu}^2)} \tag{22}$$

$$A_{X\nu} = \frac{a_{R\nu}}{0.5(a_{R\nu}^2 + a_{X\nu}^2)} \tag{23}$$

The secondary impedance

$$Z_{2\nu} = z_\nu \frac{w}{(\tau/\nu)} k_{z\nu} = (A_{R\nu} + jA_{X\nu})\nu \times \frac{w}{\tau} k_{z\nu} \frac{k_\nu}{\sigma} \coth(\kappa_\nu d/2) \tag{24}$$

where $k_{z\nu}$ = the impedance increase factor due to transverse currents [19] along the pole pitch τ.

As

$$\operatorname{ctgh}(\kappa_\nu d/2) = \operatorname{Re}[\coth(\kappa_\nu d/2)] + j \operatorname{Im}[\coth(\kappa_\nu d/2)] = A_\nu + jB_\nu$$

it is obvious that

$$Z_{2\nu} = [A_{R\nu} A_\nu + A_{X\nu} B_\nu + j(A_{X\nu} A_\nu - A_{R\nu} B_\nu)]\nu \frac{w}{\tau} k_{z\nu} \frac{k_\nu}{\sigma} \tag{25}$$

where

$$A_\nu = \sinh(a_{R\nu} k_\nu d)/[\cosh(a_{R\nu} k_\nu d) - \cos(a_{X\nu} k_\nu d)] \tag{26}$$

$$B_\nu = -\sin(a_{X\nu} k_\nu d)/[\cosh(a_{R\nu} k_\nu d) - \cos(a_{X\nu} k_\nu d)] \tag{27}$$

In the case of an aluminium secondary with thickness $d = -5$ mm and electric conductivity $\sigma = 30 \times 10^6$ S/m, the coefficients a_{Rv}, a_{Xv}, A_v, B_v for $f = 50$ Hz, $\tau = 50$ mm, $v = 1$ and $\mu_{rs} = 1$ plotted against the slip s are shown in Fig. 4.

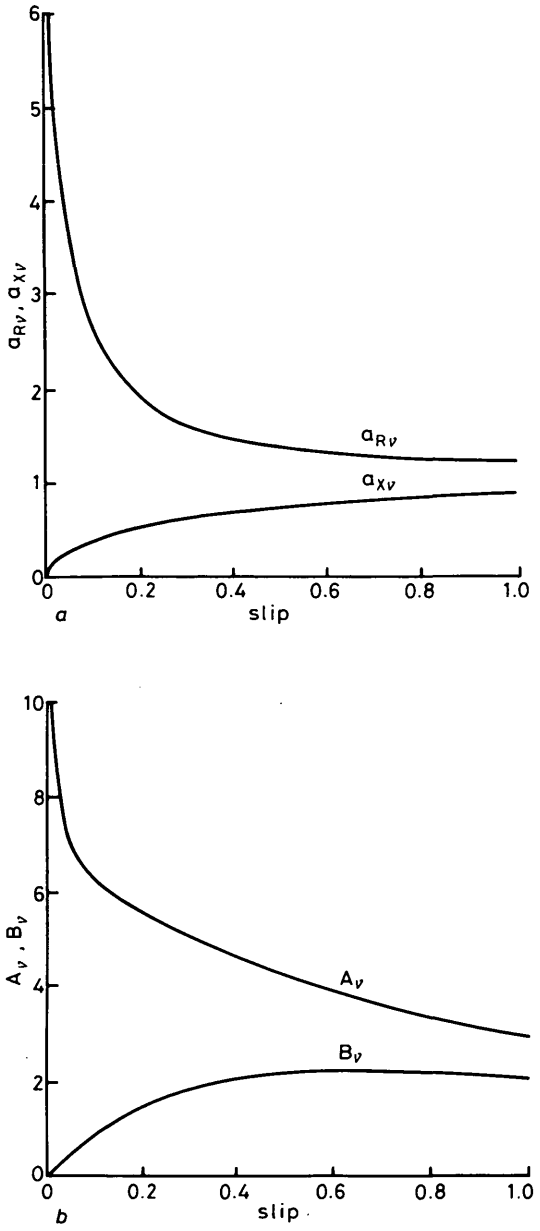

Fig. 4 *Coefficients a_{Rv}, a_{Xv}, A_v and B_v against slip for a DLIM with a homogeneous aluminium secondary*
$d = 5$ mm $\sigma = 30 \times 10^6$ S/m
$f = 50$ Hz $\tau = 0.05$ m
$v = 1$
a coefficients a_{Rv}, a_{Xv}
b coefficients A_v, B_v

Omitting the skin effect, the secondary impedance is given by

$$Z_{2v} = (a_{Rv} + ja_{Xv})v \frac{w}{\tau} k_{zv} \frac{1}{\sigma d} \tag{28}$$

Comparing eqns. 25 and 28 we have:

(i) for resistance and active power losses,

$$d'_{Rv} = a_{Rv}/(A_{Rv}A_v + A_{Xv}B_v)k_v \tag{29}$$

(ii) for reactance and reactive power losses,

$$d'_{Xv} = a_{Xv}/(A_{Xv}A_v - A_{Rv}B_v)k_v \tag{30}$$

where d'_v = equivalent thickness of the secondary taking into account the skin effect in eqn. 28. If $s = 1$, $v = 1$, $f = 50$ Hz, $\sigma = 30 \times 10^6$ S/m, $\mu_{rs} = 1$, $\tau = 50$ mm, $d = 5$ mm then $d'_R = 3.278$ mm for resistance and $d'_X = 6.498$ mm for reactance.

The resistance and reactance of the secondary reduced to the primary winding have, for $v = 1$, the following simple form:

$$R'_2 = ka_{Rv=1} \frac{w}{\tau\sigma d'_R} k_{zv=1} \tag{31}$$

$$X'_2 = ka_{Xv=1} \frac{w}{\tau\sigma d'_X} k_{zv=1} \tag{32}$$

where k comes from eqn. 3. As $d'_R < d'_X$ it is obvious that $R'_2 > X'_2$.

3.2 DLIM with short primary

The assumptions of Section 3.1 are also valid in the following considerations, but, of course, the coefficients $a_R = a_X = 1$ and $v = 1$. The model of DLIM with the short primary is shown in Fig. 5. The primary winding placed in

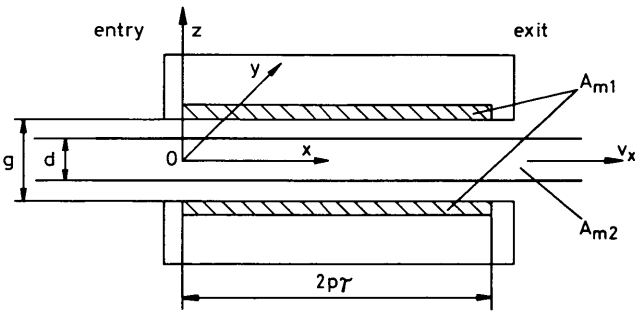

Fig. 5 *DLIM with a short secondary*

slots is represented by the two current sheets whose thickness is infinitesimally small. The peak line-current density of the primary (two inductors) is equal to

$$A_{m1} = m_1 N_1 k_{w1} \sqrt{2} I_1 / p\tau \tag{33}$$

where I_1 = RMS current input of the two inductors, the windings of which are in parallel. However, the peak line-current density of the secondary is

$$A_{m2} = \sigma d' E_{myv=1} = \sigma[(d'_R)^2 + (d'_X)^2]^{1/2} E_{myv=1} \tag{34}$$

where $E_{myv=1}$ comes from eqn. 9. As d' takes into account the skin effect, the one-dimensional field analysis presented by Yamamura [5, 6] may be applied. Then the electromagnetic field varies only in the x-direction. The differential equation of the magnetic-flux-density-normal-component distribution in the airgap has the following form:

$$\frac{g}{\mu_0} \frac{d^2 B_{mz}}{dx^2} - v\sigma d' \frac{dB_{mz}}{dx} - j\omega\sigma d' B_{mz} = j \frac{\pi}{\tau} A_{m1} \exp\left[j\left(\omega t - \frac{\pi}{\tau} x \right) \right] \tag{35}$$

Solution of eqn. 35 gives three waves travelling in the airgap, i.e. a wave travelling at synchronous speed in the positive x-direction and two so-called end-effect waves.

Proceeding analogously to References 5, 6, one obtains the electromagnetic thrust of DLIM in a form of the sum

$$F_e = F_s + F_{end} \tag{36}$$

Here F_s is the electromagnetic thrust due to the fundamental travelling sinusoidal wave at synchronous speed, and

F_{end} is the thrust caused by the core discontinuity at the entry end.

3.3 Squirrel-cage secondary

To determine the thickness d'_R of an equivalent homogeneous secondary corresponding to the squirrel cage, one can compare eqns. 1 and 31 for $s = 1$, omitting, of course, the factor k from eqn. 3. On the basis of these relationships, the equivalent thickness d'_R is

$$d'_R = \frac{a_{Rv=1}\, wN_b k_{zv=1}}{\sigma\Lambda_b\left(R_b + 2R_c + 2R_l \dfrac{1}{4\sin^2(\pi/2p)}\right)} \tag{37}$$

For $w = 0.12$ m, $\tau = 0.0501$ m, $k_{zv=1} = 1 + 2\tau/\pi w = 1.2658$, $a_{Rv=1} = 1.09$, $\Lambda_b = 2.4$ m, $N_b = 257$, $\sigma = 47 \times 10^6$ S/m, $R_b = 1.48 \times 10^{-4}$ Ω, $R_l = 6.663 \times 10^{-5}$ Ω, $2R_c = 9.2 \times 10^{-4}$ Ω and $p = 2$, one obtains $d'_R = 0.34 \times 10^{-3}$ m. To find the real thickness d of a homogeneous secondary according to eqn. 29, it is necessary to use an interative method. After calculations $d \approx 0.6 \times 10^{-3}$ m.

4 Comparison of test and calculated results

The validity of the equations given in the Section 3 was checked using the DLIM shown in Fig. 1 (the data is given in Appendix 8.1). Fig. 6 displays the load curves, i.e. the

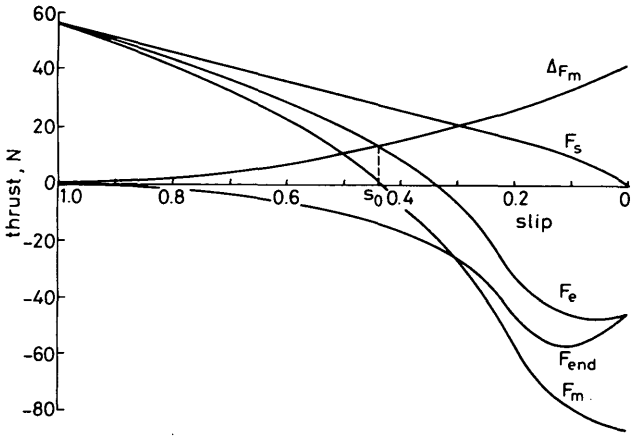

Fig. 6 *Load curves obtained from electromagnetic field theory of squirrel-cage DLIM shown in Fig. 1*

dependence of forces (eqns. 4, 5, 36) on slip, calculated on the basis of electromagnetic field theory including the end effects presented in this paper. The electromagnetic and mechanical thrust against slip, obtained on the basis of the classical theory and equivalent circuit (Appendix 8.3), is shown in Fig. 7. The calculated and measured performance characteristics are shown in Figs. 8 and 9. No-load characteristics are given in Fig. 10 and short-circuited characteristics are presented in Figs. 11 and 12. The test values agree reasonably well with the predicted curves. However, the curves calculated with the aid of the classical method are somewhat nearer to the experimental curves (apart from the short-circuit characteristics, see Fig. 11). This only occurs in the case of squirrel-cage secondary. When

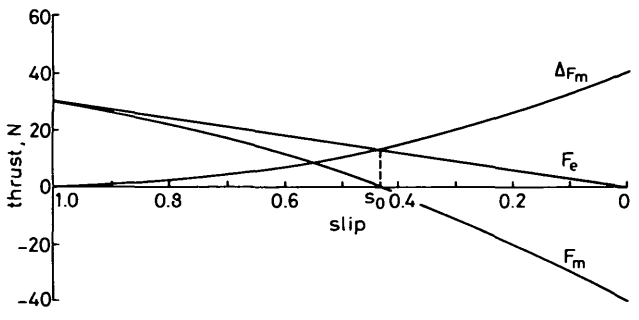

Fig. 7 *Electromagnetic F_e and mechanical thrust F_m obtained from classical theory as a function of slip*
DLIM shown in Fig. 1

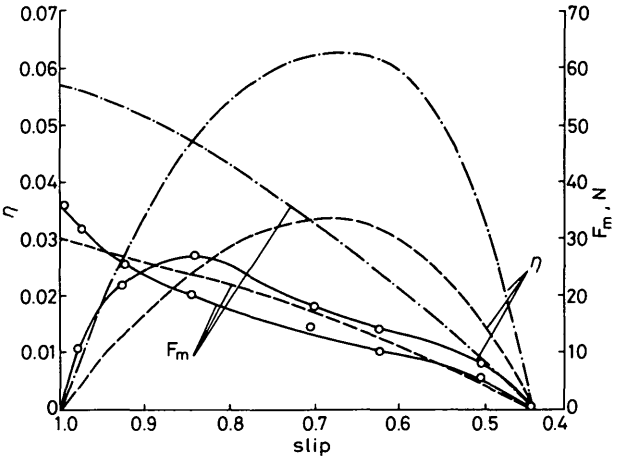

Fig. 8 *Thrust F_m and the efficiency η plotted against slip DLIM shown in Fig. 1*
——— measurements
– – – – calculations on the basis of equivalent circuit
–·–·– calculations on the basis of electromagnetic field theory

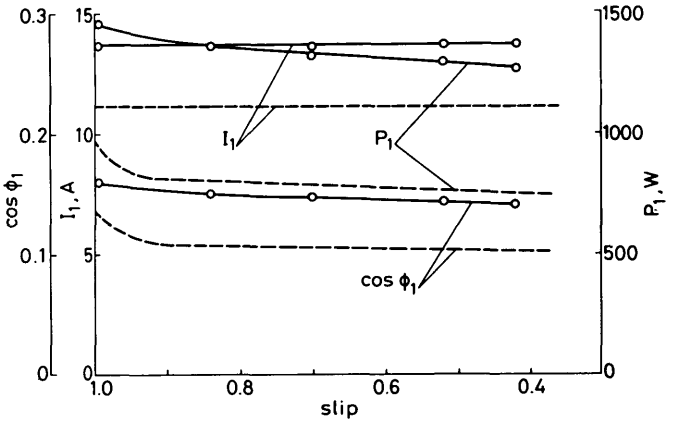

Fig. 9 *Primary current I_1 (RMS), the input power P_1 and the power factor $\cos\phi_1$ plotted against slip*
DLIM shown in Fig. 1
——— measurements
– – – – calculations on the basis of equivalent circuit

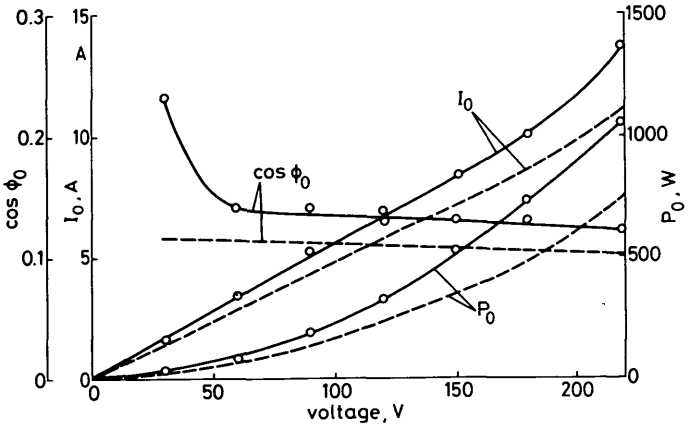

Fig. 10 *No-load characteristics of DLIM shown in Fig. 1*
——— measurements
– – – – calculations on the basis of equivalent circuit

the homogeneous secondary is applied the field-theory method including edge effects gives better results than equivalent circuits.

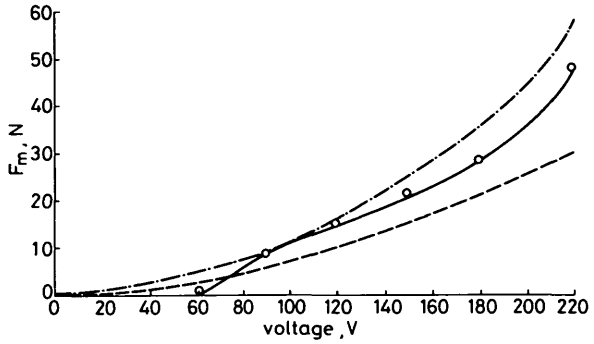

Fig. 11 *Mechanical thrust plotted against phase voltage U_1 of the DLIM shown in Fig. 1 in short circuit*

——— measurements
– – – – calculations on the basis of equivalent circuit
– · – · – calculations on the basis of electromagnetic field theory

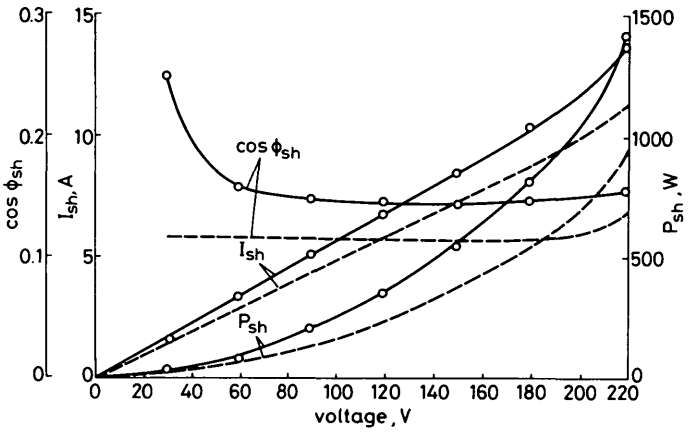

Fig. 12 *Power input P_{sh}, current I_{sh} and power factor cos ϕ_{sh} in short circuit of the DLIM shown in Fig. 1 as functions of phase voltage*

——— measurements
– – – – calculations on the basis of equivalent circuit

5 Conclusions

DLIM with squirrel-cage secondary is so complicated in its geometry that an exact solution of Maxwell's equations is quite impracticable. An approximate solution of these equations for an idealised model is obtained in this paper. This approach, owing to its simplicity, has a cognitive and practical significance. The simplified theory is very effective in analysing the DLIM and in calculating its peformances.

The thrust force indicates that the squirrel-cage DLIM performance is similar to that classically associated with the conventional DLIM with a homogeneous nonmagnetic secondary. A satisfactory correlation is obtained between the characteristics obtained analytically and experimentally. The equivalent circuit gives a mechanical thrust F_m against slip curve (Fig. 8) that is closer to the test results than the electromagnetic field theory. However, the curve of short-circuit thrust F_m coming from the electromagnetic field theory agrees better with the experimental data than the F_m curve calculated on the basis of the equivalent circuit (Fig. 11). The new equations (Section 3) will enable designers to predict confidently the performance of DLIM with squirrel-cage air-core secondary.

6 Acknowledgment

The author would like to thank R. Piekuś, M. Syroczyński and T. Zeligowski for their help in constructing the experimental machine and in calculating the performance characteristics.

7 References

1 EASTHAM, T.R., and KATZ, M.R.: 'The operation of a single-sided linear induction motor with squirrel-cage and solid-steel reaction rail' *IEEE Trans.*, 1980, **MAG-16,** pp. 722–724
2 LAITHWAITE, E.R., TIPPING, D., and HESMONDHALGH, D.E.: 'The application of linear induction motors to conveyors', *Proc. IEE*, 1960, **107A,** (6), pp. 284–294
3 LAITHWAITE, E.R.: 'Induction machines for special purposes' (George Newnes, 1966)
4 NASAR, S.A., and BOLDEA, I.: 'Linear motion electric machines' (John Wiley and Sons, 1976)
5 YAMAMURA, S.: 'Theory of linear induction motors' (University of Tokyo Press, 1972)
6 YAMAMURA, S., ITO, H., and ISHIKAWA, Y.: 'Theories of the linear induction motor and compensated linear induction motors', *IEEE Trans.*, 1972, **PAS-91,** pp. 1700–1710
7 SCHIEBER, D.: 'Principles of operation of linear induction devices', *Proc. IEEE*, 1973, **61,** pp. 647–656
8 HOLLEY, H.J., NASAR, S.A., and DEL CID, L.: 'Computations of fields and forces in a two-sided linear induction motor', *IEEE Trans.*, 1973, **PAS-92,** pp. 1310–1315
9 DUKOWICZ, J.K.: 'Theory of optimum linear induction motors', *J. Appl. Phys.*, 1976, **47,** pp. 3690–3696
10 OBERRETL, K.: 'Dreidimensionale Berechnung des Linearmotors mit Berücksichtigung der Endeffekte und der Wicklungsverteilung', *Arch. Elektrotech.*, 1973, **55,** pp. 181–190
11 YOSHIDA, K., and NONAKA, S.: 'Space harmonic analysis of short-primary linear induction machines using the Green's functions', *Mem. Fac. Eng. Kyushu Univ.*, 1976, **36,** pp. 101–138
12 YOSHIDA, K.: 'New transfer-matrix theory of linear induction machines, taking into account longitudinal and transverse ferromagnetic end effects', *IEE Proc. B, Electr. Power Appl.*, 1981, **128,** (5), pp. 225–236
13 NASAR, S.A.: 'Electromagnetic fields and forces in a linear induction motor, taking into account edge effects', *Proc. IEE*, 1969, **116,** (4), pp. 605–609
14 PRESTON, T.W., and REECE, A.B.J.: 'Transverse edge effects in linear induction motors', *ibid.*, 1969, **116,** (6), pp. 973–979
15 PIERSON, E.S., HANITSCH, R., HÜRNS, T., and MOSEBACH, H.: 'Predicted and measured finite-width effects in linear induction machines', *IEEE Trans.*, 1977, **PAS-96,** pp. 1081–1086
16 HANITSCH, R.: 'Beitrag zur Jochfluss-Verteilung in asynchronen Linearmotoren', Arch. Elektrotech., 1976, **58,** pp. 47–51
17 DELEROI, W.: 'Das Verhalten freier Ausgleichs-Wanderwellen am Beispiel eines Linearmotors', *ibid.*, 1978, **60,** pp. 87–94
18 GIERAS, J.F.: 'Analytical method of calculating the electromagnetic field and power losses in ferromagnetic halfspace, taking into account saturation and hysteresis', *Proc. IEE*, 1977, **124,** (11), pp. 1098–1104
19 GIERAS, J.: 'Theory of induction machines with double-layer secondary', *Rozpr. Elektrotech.*, 1977, **23,** pp. 577–631

8 Appendixes

8.1 Data of belt conveyor model with DLIM

8.1.1 Single primary:
number of phases, $m_1 = 3$
frequency, $f = 50$ Hz
number of pole pairs, $p = 2$
voltage betweeen phases, $U_1 = 380$ V (star)
number of slots = 12
number of coils in slots = 2
number of series-connected turns, $N_1 = 490$
winding factor, $k_{w1} = 1$
number of pairs of currents paths = 1
diameter of wire = 0.0011 m
lamination width in the y-direction = 0.10 m
pole pitch, $\tau = 0.0501$ m
tooth pitch = 0.0167 m
semi-closed slot width = 0.0102 m
slot opening = 0.0025 m
slot depth = 0.0431 m

8.2.2 Squirrel cage secondary:
bar diameter = 0.0047 m
bar length, $w = 0.12$ m
number of bars, $N_b = 257$
belt length, $\Lambda_b = 2.4$ m
braided-line cross-section = 3×10^{-6} m^2
Thickness of the secondary including woven plastics filaments = 0.0085 m

8.3.3 Airgap:
Airgap between the primary cores, $g = 0.013$ m

8.2 Electromagnetic field eqns. 9, 10, 11
Fig. 3 shows the infinite-length model of DLIM. The magnetic-flux-density space distribution in the airgap has the series form:

(i) for the upper inductor

$$B_z(x) = \sum_{\nu=1}^{\infty} B_{m\nu} \exp(-j\beta_\nu x) \tag{38}$$

(ii) for the lower inductor (Section 3.1, assumption (*b*))

$$B_z(x) = \sum_{\nu=1}^{\infty} B_{m\nu} \exp[-j\beta_\nu(x + x_0)] \tag{39}$$

Using the magnetic vector potential

$$\nabla \times \boldsymbol{A} = \boldsymbol{B} \tag{40}$$

the second Maxwell's equation

$$\nabla \times \boldsymbol{E} = -\frac{\partial \boldsymbol{B}}{\partial t} \tag{41}$$

and the assumptions (*c*), (*g*), and (*i*), for two-dimensional field distribution one obtains:

$$E_{my} = -j\omega A_{my} \tag{42}$$

$$B_{mx} = -\frac{\partial A_{my}}{\partial z} \tag{43}$$

$$B_{mz} = \frac{\partial A_{my}}{\partial x} \tag{44}$$

$$\frac{\partial^2 A_{myv}}{\partial x^2} + \frac{\partial^2 A_{myv}}{\partial z^2} = \alpha_\nu^2 A_{myv} \tag{45}$$

The magnetic vector potential

$$A_{my}(x, z) = \sum_{\nu=1}^{\infty} A_{myv}(x, z)$$

is assumed to be y-directed and is not a function of y. The functions $A_{myv}(x, z)$ satisfy Helmholtz's eqn. 45. Magnetic vector potential can be written as

$$A_{my} = \sum_{\nu=1}^{\infty} \exp(-j\beta_\nu x) \times [C_{1\nu} \exp(-\kappa_\nu z) + C_{2\nu} \exp(\kappa_\nu z)] \tag{46}$$

In deriving eqn. 46 from eqn. 44, the solution for normal component of magnetic flux density inside the secondary has the form

$$B_{mz} = -\sum_{\nu=1}^{\infty} j\beta_\nu \exp(-j\beta_\nu x) \times [C_{1\nu} \exp(-\kappa_\nu z) + C_{2\nu} \exp(\kappa_\nu z)] \tag{47}$$

To evaluate the constants $C_{1\nu}$, $C_{2\nu}$, the following boundary conditions are used:

$$B_{m\nu} = -j\beta_\nu[C_{1\nu} \exp(-\kappa_\nu d/2) + C_{2\nu} \exp(\kappa_\nu d/2)] \quad \text{for } z = \frac{d}{2}$$

$$B_{m\nu} \exp(-j\beta_\nu x_0) = -j\beta_\nu[C_{1\nu} \exp(\kappa_\nu d/2) + C_{2\nu} \exp(-\kappa_\nu d/2)] \quad \text{for } z = -\frac{d}{2}$$

From these conditions and with the aid of eqns. 38, 39 and 47 one obtains:

$$C_{1\nu} = j \frac{B_{m\nu}}{2\beta_\nu \sinh(\kappa_\nu d)} \times [\exp(\kappa_\nu d/2) \exp(-j\beta_\nu x_0) - \exp(-\kappa_\nu d/2)] \tag{48}$$

$$C_{2\nu} = j \frac{B_{m\nu}}{2\beta_\nu \sinh(\kappa_\nu d)} \times [\exp(\kappa_\nu d/2) - \exp(-\kappa_\nu d/2) \exp(-j\beta_\nu x_0)] \tag{49}$$

In case of $x_0 = 0$

$$C_{1\nu} = C_{2\nu} = j \frac{B_{m\nu}}{\beta_\nu \sinh(\kappa_\nu d)} \sinh(\kappa_\nu d/2) \tag{50}$$

Substituting eqn. 50 into eqns. 46 and 47, and utilising eqns. 42 and 43 we obtain eqns. 9, 10, 11, in which the displacement $x_0 = 0$.

8.3 Equivalent circuit of DLIM
The theory of an induction motor is usually presented in one of two ways: either the analytical expressions are derived from electromagnetic field theory, or the machine is represented by an equivalent circuit. It is often convenient to consider not a real DLIM, but an equivalent electrical system, for example, as in Fig. 13*a*. It is necessary to note that the entry and exit edge effects are neglected in the circuital methods of LIM analysis. With the equivalent circuit presented in Fig. 13*a* we can transform to the

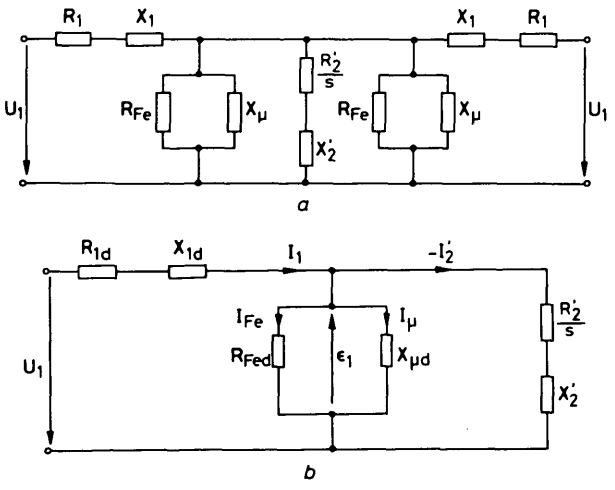

Fig. 13 *T-type equivalent circuit of DLIM excluding edge effects*
a windings of two inductors in parallel
b transformed equivalent circuit

simpler form shown in Fig. 13*b*, where $R_{1d} = 0.5R_1$, $X_{1d} = 0.5X_1$, $R_{Fed} = \varepsilon_1/I_{Fe}$, $X_{\mu d} = \varepsilon_1/I_\mu$ and $I_0 = I_{Fe} + jX_\mu$ (no-load current). The resistance R'_2 and reactance X'_2 are obtained from eqns. 31 and 32, respectively, in which $s = 1$. Formulas for the resistance R_1 and the inductive leakage reactance X_1 of the primary are well known.